Propagation of wiggler focused relativistic sheet electron beams

J. H. Booske, W. W. Destler, Z. Segalov, D. J. Radack, E. T. Rosenbury, J. Rodgers, T. M. Antonsen, Jr., V. L. Granatstein, and I. D. Mayergoyz
Laboratory for Plasma and Fusion Energy Studies, University of Maryland, College Park, Maryland 20742

(Received 24 November 1987; accepted for publication 9 February 1988)

A recent design concept for millimeter-wave free-electron lasers [J. Appl. Phys. **60**, 521 (1986)] would require the stable propagation of a sheet electron beam through a narrow waveguide channel. Experimental results reported in this article support the feasibility of such a configuration by demonstrating the stable propagation of relativistic sheet electron beams through a narrow waveguide gap (3.2 mm) using focusing by a short-period electromagnet wiggler. 90% of the electron current in a 100-keV sheet electron beam was transmitted through a 5-cm-long channel with peak wiggler fields of 800 G. Almost 80% of a 400-keV beam was similarly confined with a 1600-G wiggler field. The data were consistent with single electron trajectory models, indicating that space-charge effects were minimal. No evidence of beam breakup or filamentation instabilities was observed.

I. INTRODUCTION

Sheet or ribbon electron beams, as opposed to solid cylindrical electron beams, have attractive features for a number of applications. For example, it has been noted[1] that microwave tubes employing sheet beams might carry higher currents than those with solid beams, since sheet beam currents would not be limited in perveance (current is increased by increasing the width of the beam). Furthermore, sheet beams could carry these high currents and yet be thin enough to permit good coupling with small-scale millimeter-wave circuits.[1–4] Achieving higher currents in small rf structures is also facilitated by somewhat higher space-charge current limits on flat sheet beams propagated between parallel conducting plates, as opposed to solid beams or thin annular beams located near conducting walls.[4] Converting from cylindrical solid to sheet beams may permit substantial reduction in space-charge effects on the efficiency of devices in which electron energy is recovered.[5] Finally, it has been noted that sheet electron beams are well suited for gas laser excitation[6] and plasma chemistry reactors.[7]

Interest in these possible applications and advantages has spurred theoretical and experimental studies on the generation and stable propagation of sheet beams. To prevent beam erosion of unneutralized electron beams, of course, requires a method to focus against electrostatic repulsion forces and perhaps the simplest solution is an axial magnetic field. Unfortunately, this is an unstable configuration for sheet beams, due to $\mathbf{E}\times\mathbf{B}$ drift forces arising from the guiding magnetic field $\mathbf{B}$ and the transverse electric self-fields of the beam. The simplest instability mode of this type is a beam rotation discussed in Ref. 5. Both experiment and theory showed that this instability was suppressed—but not entirely eliminated—by placing the beam between closely spaced conducting plates and increasing the strength of the axial magnetic field.[5] A much greater body of work discusses the diocotron or filamentation instability of sheet beams in axial magnetic fields. This mode—caused by $\mathbf{E}\times\mathbf{B}$ velocity shear in the beam—has been investigated for both nonrelativistic[5,7–12] and relativistic[4,13,14] beams. The principal findings are that ion space-charge neutralization,[9] very strong magnetic fields,[4,13] highly relativistic beam velocities,[13] and closely spaced conducting boundaries,[10–12] tend to stabilize this beam-disrupting mode. On the other hand, parallel velocity shear[11,12] may lead to fine-scale perturbations of the sheet beam. These fluctuations may be stabilized by finite temperature effects.[11] At high beam densities,[14] the diocotron instability develops into macroscopic kink modes, as well as the shorter wavelength filamentation modes. Although very strong magnetic field strengths may suppress the diocotron instability, the field intensity to achieve stability may be so high that it either entirely prevents transverse electric (TE) electromagnetic instabilities (such as the free-electron laser instability),[4] or reduces their gain below that of modes having axial electric fields.[15]

Alternative methods of focusing sheet beams other than uniform axial magnetic fields involve periodic deflection focusing techniques. These include electrostatic deflection (or "slalom") focusing,[16,17] periodic longitudinal magnetic (or PPM) focusing,[18] and magnetic deflection (or wiggler) focusing.[1,2] For high current beams, the periodic magnetic schemes are generally preferable to electrostatic deflection due to breakdown field limitations and the potential for instabilities associated with the latter approach. In addition, PPM focusing is also likely to be unstable to the diocotron instability.[18] In conclusion, strong wiggler focusing would appear to be the best choice for focusing high current sheet electron beams for several reasons. First, the uncomfortably high electric fields necessary to "slalom" focus high currents can be replaced with more modest magnetic wiggler fields.[1] This advantage improves at relativistic beam velocities. Second, periodic magnetic focusing systems require smaller magnet volume to produce the same rms value of magnetic field in the vicinity of the electron beam than for uniform magnetic focusing.[1,2] Finally, wiggler focusing should be relatively immune to velocity shear instabilities (such as diocotron) due to much weaker coupling with longitudinal magnetic field components as compared with either uniform or PPM magnetic focusing.[1,2]

Recent proposals for a millimeter-wave free-electron laser (FEL) design based on small-period magnetic wigglers[19,20] will require the stable propagation of wiggler-fo-

 0021-8979/88/130006-06$02.40

cused relativistic sheet electron beams. Typical designs call for beam thicknesses of 0.5–1.0 mm and beam widths of up to 50 mm propagating in wiggler magnetic fields with periods less than or equal to 1.0 cm. To achieve high magnetic field intensities with the short-period wigglers, the gap between magnet halves (and thus the gap through which the beams must propagate) must be kept small, typically 2.5–4.5 mm. The sheet beam will be bounded above and below by parallel conducting plates, consistent with FEL electromagnetic cavity requirements.

Theory indicates that the most stable configuration for sheet beam propagation involves wiggler focusing and parallel conducting boundaries. However, very little experimental verification of this claim has been reported, especially for relativistic beams and very narrow beam channels. An experimental investigation has therefore been undertaken to study this issue.

II. THEORY

To lowest order, the fields produced by periodic wigglers of the sort described in Ref. 19 can be written as

$$\mathbf{B}_W = [0, B_y(y,z), B_z(y,z)] = \nabla x \mathbf{A}_W , \tag{1a}$$

$$\mathbf{A}_W = [A(y,z),0,0] , \tag{1b}$$

$$A(y,z) = (B_w/k_w)\cosh(k_w y)\cos(k_w z); \quad k_w \equiv 2\pi/l_w . \tag{1c}$$

Here, l_w is the wiggler period length.

As indicated in Fig. 1, the z axis is oriented parallel to the initial velocity of the electron beam, the y axis is oriented along the small transverse dimension of the beam, and the x axis is assumed parallel to the wide transverse dimension of the beam. In the midplane of the gap ($y = 0$), the magnetic field has only a periodic y component. This induces the periodic "wiggling" velocity v_{wx} of an electron in the x-z plane which leads to the FEL interaction. For nonzero values of y there is also a periodic z component of magnetic field B_{wz} which increases in intensity as one approaches the magnet faces. This axial field component acts upon the wiggling velocity v_{wx} so that electrons displaced from the $y = 0$ plane experience an inward focusing force. For convenience, this focusing force can be related to the inhomogeniety of the wiggler field as[20]

$$F = -\nabla \frac{m}{2\gamma}\left\langle\left(\frac{qA}{m}\right)^2\right\rangle \approx \frac{m}{4\gamma}\left(\frac{\Omega_w}{k_w}\right)^2 \nabla \cosh^2(k_w y) , \tag{2}$$

where $\Omega_w = qB_w/m$, the brackets $\langle\rangle$ indicate an average over a wiggler period, and $\gamma = [1 - (v_0/c)^2]^{-1/2}$ is the relativistic energy parameter. If we assume a beam which is modeled by a flat density profile in y [i.e., $n(x,y,z) \approx n(x)$ for $|y| \leq \Delta/2$, where Δ is the beam thickness] and assume that the electrostatic self-fields are greatest in the y dimension (i.e., $E_y \geq E_x$), then Poisson's equation can be combined with Eq. (2) to find conditions for period-averaged beam confinement in the y dimension. For very thin sheet beams, the hyperbolic cosine dependence in Eq. (2) can be expanded about $y = 0$ to obtain a limit on beam plasma frequency (for confinement against space-charge repulsion):

$$\omega_p < (\gamma_z/\sqrt{2\gamma})\Omega_w , \tag{3}$$

where $\omega_p^2 = 4\pi n e^2/m_e$ and $\gamma_z = [1 - (v_z/c)^2]^{-1/2}$. Pinch forces due to the beam's self-magnetic field have also been included in the derivation of Eq. (3).

Satisfaction of Eq. (3) is a necessary, but not sufficient, condition to prevent beam current from intercepting the waveguide walls. A second condition arises from consideration of single particle motions in the y-z plane. For small values of $k_w y$, Eq. (2) can be approximately written as

$$\ddot{y} \simeq -(1/2\gamma^2)\Omega_w^2 y . \tag{4}$$

For initial conditions $y(t = 0) \simeq 0$ and $dy/dt(t = 0) = v_{y0}$, one can solve Eq. (4) for the "betatron" motion:

$$y(z) \simeq Y_0 \theta_0 \sin(\Omega_w z/\gamma\sqrt{2}\beta_{z0}c) , \quad Y_0 \equiv (\gamma\sqrt{2}\beta_{z0}c/\Omega_w) , \tag{5}$$

where it has been assumed that $z \simeq v_{z0}t = \beta_{z0}ct$, and $\theta_{y0} = v_{y0}/v_{z0}$ is a pitch angle at injection. To avoid beam current "scrape-off" in the waveguide channel, the maximum betatron amplitude must be less than half of the small transverse waveguide dimension; i.e., $y_{max} < b_{rf}/2$ (cf. Fig. 1). This imposes a maximum limit on the injected pitch angle θ_{y0}:

$$\theta_{y0} < \theta_{crit}$$

$$\theta_{crit} \approx \begin{cases} b_{rf}/2L, & L/Y_0 < 0.1 \\ \dfrac{b_{rf}}{2Y_0 \sin(L/Y_0)}, & 0.1 < L/Y_0 \leq \pi/2 \\ \dfrac{b_{rf}}{2Y_0}, & L/Y_0 > \pi/2, \end{cases} \tag{6}$$

where L is the length of the wiggler/waveguide region.

For the experiments described in this paper, no attempt was made to confine the beam in the horizontal (x-z) plane. Instead, these measurements were restricted to relatively short wigglers with relatively wide waveguide channels (the important issue of horizontal confinement will be investigated in future planned experiments). Consequently, the dy-

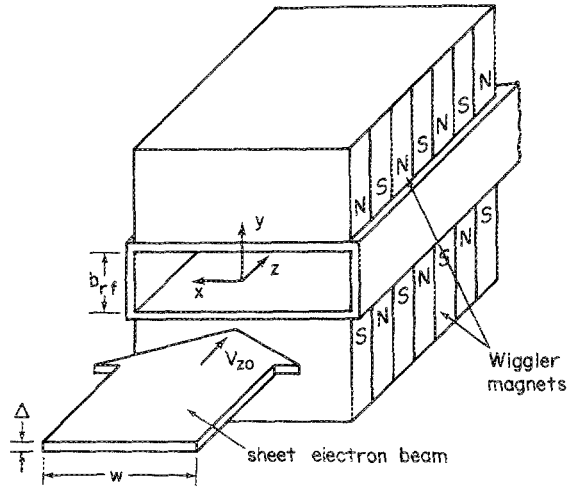

FIG. 1. Geometry for propagation of a wiggler-focused sheet electron beam in a narrow waveguide channel.

namics of electrons in the horizontal plane of the wiggler gap had to be analyzed for a proper interpretation of the data. For an idealized wiggler having the periodic (with uniform amplitude) fields of Eq. (1) and being infinitely wide in the x dimension, the single electron Lagrangian is independent of x. Consequently, conjugate canonical momentum in the x direction is conserved; viz.,

$$m\gamma c\beta_x(z) + (q/c)A_x(z) = m\gamma c\beta_x(z=-\infty) + (q/c)A_x(z=-\infty)\,. \quad (7)$$

Averaging over an integral number of wiggler periods, assuming that the wiggler fields begin abruptly at $z=0$, and assuming that electrons are injected parallel to the z axis (no initial x velocity), one finds that electrons undergo a constant drift in the x-z plane; viz.,

$$\langle\beta_x\rangle = a_w/\gamma\,, \quad (8)$$

where $a_w = qB_w/(k_w c^2)$ is the wiggler pump parameter and the brackets denote an average over the wiggle motion. Physically, Eqs. (7) and (8) state that the (period-averaged) horizontal drift is proportional to the (period-averaged) difference in magnetic flux between the electron's position z and the point of injection ($z=-\infty$). For cases where $a_w^2 \ll 1$, this horizontal drift can be related to a deflection angle $\theta_h \simeq \arcsin(\langle\beta_x\rangle/\beta_{z0})$ as illustrated in Fig. 2. Consequently, the amount of horizontal displacement observed for beam electrons exiting the end of the wiggler will depend on the peak field strength B_0 and the electron energy, γ.

Image charges in the (grounded) conducting waveguide walls substantially reduce the space-charge forces acting in the x direction.[20] Collective electrostatic effects on electron dynamics in the x-z plane were therefore ignored in the experimental data analyses discussed later in this paper.

III. EXPERIMENTAL CONFIGURATION

The experiments were performed with a pulse line accelerator[21] and a cold cathode. Cathode, anode, and diode gap dimensions were chosen to ensure that diode operation would approximate that of a planar diode. Ideally, it would have been preferable to generate a sheet beam by machining a rectangular slit aperture in the stainless-steel anode. However, there was concern that such a configuration would permit poor beam quality in the x dimension due to nonuniform cathode emission and/or self-pinching effects in the diode region. As a compromise, we chose to generate a set of horizontally spaced round beamlets as depicted in Fig. 3. Subsequent experiments verified that these beamlets spread out horizontally to form a continuous sheet soon after entry into the channel.

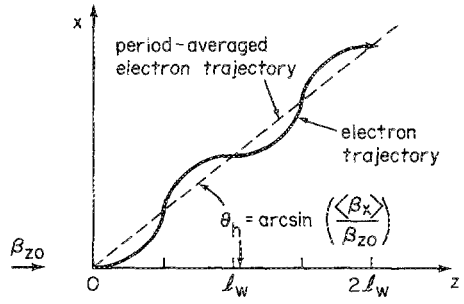

FIG. 2. Horizontal drift of an electron trajectory in a planar wiggler with untapered entrance conditions.

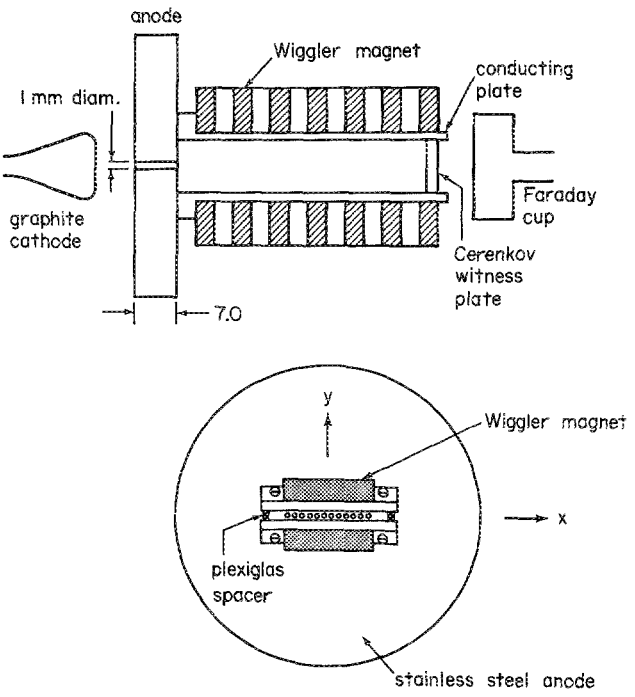

FIG. 3. Configuration for wiggler-focused sheet beam propagation studies using a pulse line accelerator and a field emission planar diode.

The wigglers employed were electromagnets of the type described in Ref. 19. For the studies reported here, the wiggler period was approximately 1.0 cm, the "waveguide" channel (gap between the conducting plates) was 3.2 mm, and the wigglers were five periods long. Seventeen 1.0-mm diam holes were drilled into the anode plate with a spacing between holes of approximately 3.0 mm. The channel spacing between the conducting plates was maintained by Plexiglas spacers and the entire assembly was enclosed in an evacuated 15.0-cm-diam stainless-steel drift tube.

Beam diagnostics included both a fast response graphite Faraday cup and an axially movable, Plexiglas Cerenkov witness plate imaged with an open-shutter graflex camera. Other diagnostic signals were also measured to monitor relevant current and voltage waveforms generated in the pulse-forming circuit.

Typical waveforms for the cathode voltage (monitored with an integrated $\dot{D}$ probe) and the Faraday cup signal are presented in Fig. 4 for a configuration in which the wiggler magnets and the conducting plates were absent.

The most pronounced feature of the current trace in Fig. 4(b) is the existence of the two current pulses, each approximately 50 ns long and separated by 50 ns. Impedance mismatch between the diode and the pulse line generator resulted in ringing of the cathode voltage. In Fig. 4(a), one can see that 50 ns after the first pulse, the cathode voltage rings negative for a second time, ejecting a second pulse of electron current. The energy of electrons in this second pulse is probably somewhat less than the indicated cathode voltage, however, due to plasma effects in the diode. Nevertheless, from

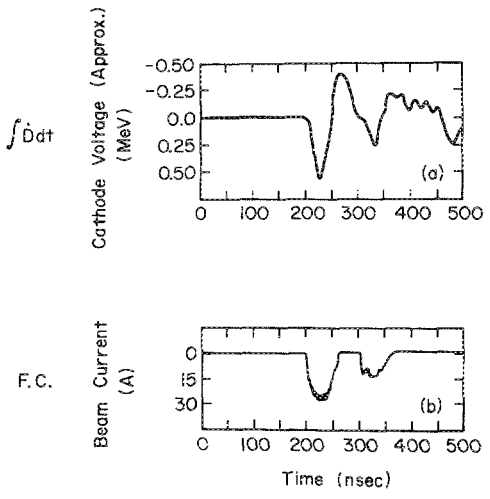

FIG. 4. Typical signal traces for the pulsed beam experiments: (a) approximate cathode voltage as monitored by an integrated $\dot{D}$ probe (calibration is 250 ± 50 keV per division), (b) electron current as measured with a graphite Faraday cup.

these two traces one can conclude that there are two pulses of electron current: one with approximately 26 A at 400–600 keV, and the second one having approximately 14 A at less than 300 keV.

Figure 5 depicts open-shutter photographs of the witness plate imaged at two different locations along the z axis of the wiggler. Figure 5(a) shows an image of the array of beamlets as they exit the anode ($z = 0$). Although film response nonlinearity prohibits an accurate estimate of the transverse current distribution from Fig. 5(a), measurements have confirmed that the majority of the injected current (approx. 26 A in the first pulse) was concentrated in the centermost 7–9 beamlets. Moving the witness plate downstream, it was observed that the individual beamlets coalesced rapidly in the horizontal (x) dimension. This effect is shown in Fig. 5(b), where at $z \approx 2.5$ cm, one observes a sheet beam image with transverse dimensions of approximately 3 mm $\times$ 30 mm.

A plot of the peak wiggler field amplitudes (normalized to the average amplitude value) versus axial position (denoted by the wiggler period number) is shown in Fig. 6. In

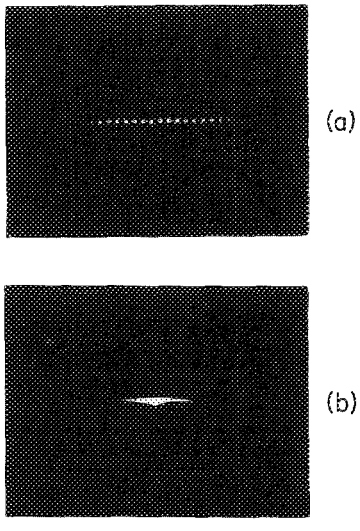

FIG. 5. Open-shutter photographs of witness plate images of the beam in the waveguide channel: (a) beam image at anode exit plane ($z = 0$), (b) beam image at $z \approx 2.5$ cm.

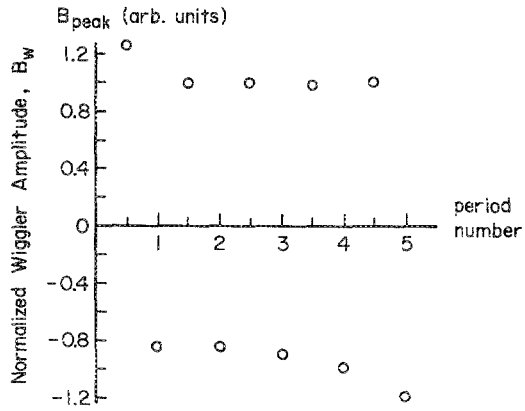

FIG. 6. Wiggler magnetic field amplitudes normalized to the average field amplitude.

the center of the magnet, the period-to-period variation in the amplitudes is small, but there is a residual 10% dc bias component superimposed on the spatially periodic field. The field in the two outermost windings is also 20% higher than the field in the magnet center. The significance of these features must be considered in light of the fact that the approximate analytic trajectory formulas discussed above were derived for idealized magnets in which all peak wiggler field amplitudes were assumed uniform. Anticipating possible difficulties with data analysis, a numerical code was developed to simulate three-dimensional single particle trajectories in arbitrarily specified electromagnetic fields. As will be discussed shortly, electron motion in the y-z plane was essentially the same for idealized (uniform peaks) wiggler fields and field profiles based on the measurements of Fig. 6. However, motion in the x-z plane was much more sensitive to the uniformity of the wiggler field. In describing the beam propagation measurements, specified values of the wiggler field amplitude will refer to the average peak value (i.e., a normalized value of 1.0 in Fig. 6). This will facilitate comparisons between theoretical predictions for the idealized and measured wiggler field profiles.

IV. RESULTS

The amount of electron current transmitted through the beam channel is plotted in Figs. 7(a) and 7(b) as a function of the (average) wiggler field amplitude. The data of Fig. 7(a) correspond to the first current pulse, whereas the data of Fig. 7(b) correspond to the second current pulse [cf. Fig. 4(b)]. In both cases it is apparent that the amount of current propagated through the channel generally increased with increasing wiggler field strength. An exception to this is noted for the second pulse where a dramatic decrease in the transmitted current was observed when wiggler fields exceeded 1.0 kG. This anomaly, as well as the theoretical predictions represented by the solid curves, will be discussed in the following section. In both figures, the representative error bars are determined from a combination of shot-to-shot variations and noise on the Faraday cup current trace.

Witness plate images of the beam cross section at the exit of the wiggler are displayed in Fig. 8 for a case with no

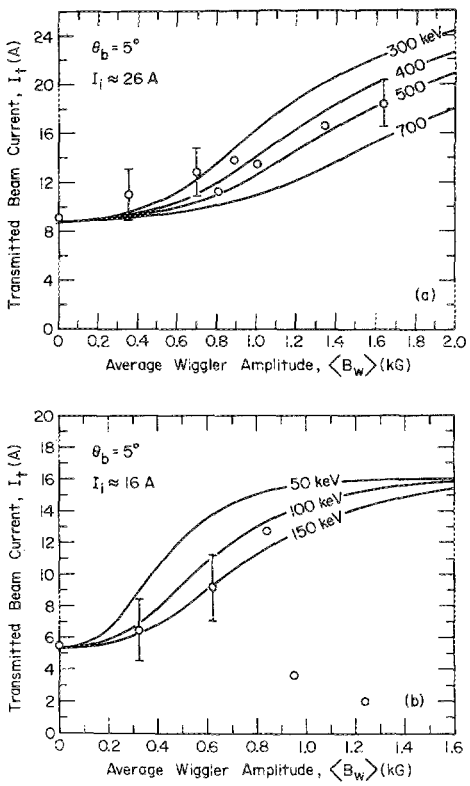

FIG. 7. Transmitted electron current vs average wiggler field amplitude: (a) for first current pulse (cf. Fig. 4), and (b) for second current pulse.

wiggler field [Fig. 8(a)] and a case with a wiggler field strength of approximately 1.5 kG. The strong focusing of the beam cross section in the vertical dimension is clearly visible. The same witness plate measurements also provided evidence of a horizontal drift as discussed in Sec. II. Data for the horizontal displacement of the first current pulse (measured at the exit of the wiggler) are displayed in Fig. 9. Again, a description of the solid curves is deferred to the next section.

V. DISCUSSION

One of the most important observations was the lack of any indication of grossly disruptive beam instabilities. Although no quantitative theoretical instability analyses were performed for these experiments, this result is consistent with existing theory[1,2,4,5,7–14,18] in that the beam is relativistic, the interaction region is relatively short and bounded by conducting plates, wiggler focusing is employed, and the current is relatively low for the beam voltage used.

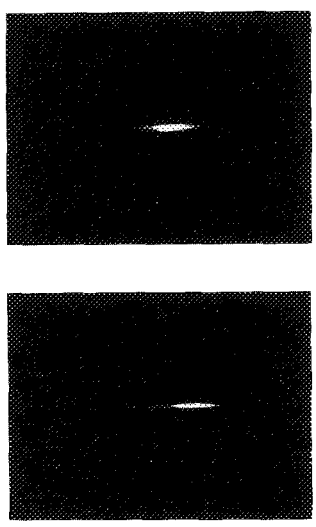

FIG. 8. Witness plate images of the beam cross section at the exit of the wiggler for: (a) no wiggler field, and (b) 1.5-kG average wiggler field amplitude.

The next issue concerns the effectiveness of the wiggler focusing. The beam envelope equation for an infinitely wide sheet beam propagating in a vacuum (no magnetic fields) with approximately constant cross section is

$$\Delta_b \approx \Delta_{b0} \exp(\omega_p z/\gamma^{3/2}\beta_{z0}c) . \tag{9}$$

For the parameters of our experiments, Eq. (9) indicates that space-charge expansion plays a negligible role in the observed loss of current through the channel. This is consistent with the fact that the relatively low beam current precludes any collective effects. Furthermore, Eq. (3) is easily satisfied by field strengths as low as 200 G. This leaves confinement of single particle trajectories as the dominant issue for beam propagation in the waveguide gap.

The dimensions of the anode beamlet aperture(s) indicated in Fig. 3 permit the passage of electron trajectories having initial pitch angles of less than or equal to approximately 8°. However, in the absence of any focusing electron pitch angles (in the y-z plane) must be less than approximately 3.5° to avoid scrape-off on the conducting plates. For an initial distribution of electron pitch angles $f(\theta)$, one would expect that the fractional current transmitted through the channel as a function of wiggler and beam parameters can be computed as

$$\frac{I_t}{I_i} = \left(\int_0^{\theta_{\rm crit}} d\theta f(\theta)\right) \Big/ \left(\int_0^{\pi/2} d\theta f(\theta)\right), \tag{10}$$

on the basis of confining the betatron amplitudes within the gap spacing b_{rf}. The maximum confined angle $\theta_{\rm crit}$ is determined from Eq. (6). I_t is the transmitted current and I_i is the injected current. To analyze the measurements reported here, a Gaussian pitch angle distribution function was assumed:

$$f(\theta) \sim \exp(-\theta^2/\theta_b^2) , \tag{11}$$

where θ_b characterizes the spread in initial pitch angles. Then from the measured values of I_i, L, b_{rf}, Eqs. (6), (10), and (11) were combined to compute a predicted value of $I_t(B_w = 0)$ as a function of θ_b. As seen in Figs. 7(a) and 7(b), agreement between theory and experiment for $I_t(B_w = 0)$ was obtained with a value of $\theta_b \approx 5°$. This is consistent with the maximum expected value of 8°. For a value of $\theta_b = 5°$, Eq. (10) was then used to calculate predicted values of transmitted current versus average wiggler field amplitude for different values of electron energy. Representative calculations are plotted as the solid curves in Fig. 7. The data in Fig. 7(a) agree well with the simplified theory for a beam electron energy between 300 and 500 keV. For wiggler field amplitudes below 1.0 kG, the data for the second current pulse [Fig. 7(b)] agree with the theory for electon energies between 100 and 150 keV. Both of these energy ranges are consistent with the previous discussion on the calibration of the cathode voltage D probe.

The measured horizontal displacement of the beam

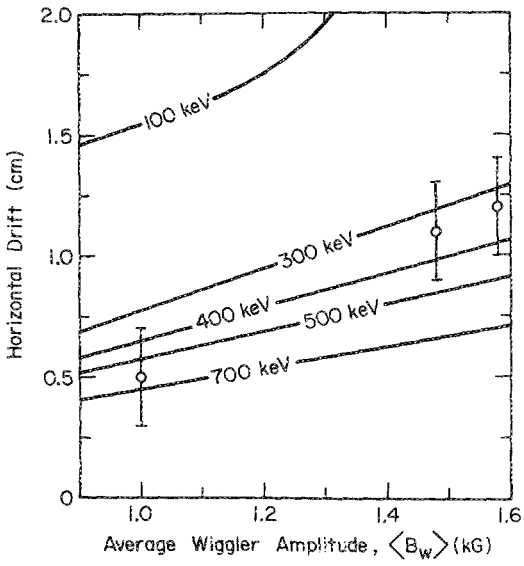

FIG. 9. Net horizontal displacement of the first current pulse as measured at the wiggler exit plane. Solid lines are single electron trajectory theory predictions using the wiggler field profile of Fig. 6.

(Fig. 9) did not agree well with the predictions of Eq. (8) assuming uniform values of wiggler field amplitude. As previously mentioned, numerical simulations indicated that the horizontal plane trajectories are sensitive to wiggler field nonuniformities such as the dc offset and the enhanced end field effects of Fig. 6. Consequently, single electron trajectories were calculated with the simulation code using magnetic field profiles based on Fig. 6. The predictions for the net horizontal displacement at the exit of the wiggler are plotted as the solid curves in Fig. 9 as a function of average wiggler field amplitude and electron energy. Again, the data for the first current pulse were found to be consistent with an energy of approximately 400 keV. On the other hand, electrons with an energy of less than or equal to approximately 100 keV were predicted to have trajectories upon exiting the wiggler that would result in their missing interception by the Faraday cup. This would explain the decrease of measured transmitted current in Fig. 7(b) above 0.8 kG.

VI. CONCLUSIONS

Wiggler focusing of relativistic sheet electron beams in narrow waveguide channels has been demonstrated for beams with energies of approximately 100 and 400 keV, and a wiggler having five periods with a period length of 1.0 cm. Individual beamlets with diameters of 1.0 mm were shown to merge in the channel into a sheet beam approximately 30 mm wide. For an average wiggler field amplitude of 1.6 kG, approximately 77% of the injected 400-keV beam current was recovered. This is compared with only 35% transmission of the unfocused 400-keV beam. Nearly 90% of the current in the 100-keV beam was transmitted at wiggler fields of 0.8 kG versus only 34% transmission without any wiggler focusing.

The transmitted current data were in good agreement with theoretical predictions based on confinement of single electron betatron trajectories in the small transverse dimension. Beam displacement in the large transverse dimension was also in good agreement with single electron dynamics, provided experimental wiggler field nonuniformities were properly accounted for. Higher percentages of transmitted current will require larger wiggler fields, reduction of wiggler field nonuniformities, and possibly tighter constraints on the pitch angle spread of the injected electron beam. No evidence of beam breakup or filamentation instabilities was observed.

ACKNOWLEDGMENTS

The authors would like to acknowledge the helpful discussions with Dr. B. Levush. Technical assistance from W. Crowe, J. Pyle, D. Cohen, and M. Reagan was also appreciated. This work was supported by SDIO/IST through a contract administered by ONR, and by the Department of Energy.

[1]P. A. Sturrock, J. Electron. Contr. **7**, 162 (1959).
[2]V. W. Dryden, Ph.D. dissertation (Dept. of Electrical Engineering, Stanford University, University Microfilms Intl. Ann Arbor, MI, 1960).
[3]R. M. Phillips, IRE Trans. Electron. Devices **ED-7**, 231 (1960).
[4]G. Providakes, J. A. Nation, an M. E. Read, IEEE Trans. Micro. Theory Tech. **25**, 563 (1977).
[5]V. A. Lebedev, I. N. Meshkov, and A. N. Sharapa, Sov. Phys. Tech. Phys. **24**, 421 (1979).
[6]R. K. Bevov, V. S. Mezhevov, Yu. B. Smakovskii, and A. P. Strel'tsov, Instrum. Expt. Tech. **18**, 697 (1975).
[7]H. F. Webster, J. Appl. Phys. **26**, 1386 (1955).
[8]C. C. Cutler, J. Appl. Phys. **27**, 1028 (1956).
[9]R. L. Kyhl and H. F. Webster, IRE Trans. Electron. Devices **3**, 172 (1956).
[10]J. R. Pierce, IRE Trans. Electron. Devices **3**, 183 (1956).
[11]T. M. Antonsen, Jr. and E. Ott, Phys. Fluids **18**, 1197 (1975).
[12]V. G. Leiman, A. A. Tevryukov, A. P. Ovchinnikov, and G. N. Freiber, Sov. J. Plasma Phys. **4**, 377 (1978).
[13]B. G. Leiman, O. B. Ovsyannikova, and I. D. Rodionov, Sov. J. Plasma Phys. **10**, 70 (1984).
[14]H. C. Chen, IEEE Trans. Nucl. Sci. **32**, 2380 (1985).
[15]N. S. Ginzburg and Yu. V. Novozhilova, Sov. Phys. Tech. Phys. **28**, 1037 (1984).
[16]J. S. Cook, R. Kompfner, and W. H. Yocum, Proc. IRE **45**, 1517 (1957).
[17]P. T. Kirstein, G. S. Kino, and W. E. Waters, *Space-Charge Flow* (McGraw-Hill, New York, 1967).
[18]G. Dohler, IEEE Trans. Electron Devices **28**, 602 (1981).
[19]W. W. Destler, V. L. Granatstein, I. D. Mayergoyz, and Z. Segalov, J. Appl. Phys. **60**, 521 (1986).
[20]V. L. Granatstein, T. M. Antonsen, Jr., J. H. Booske, W. W. Destler, P. E. Latham, B. Levush, I. D. Mayergoyz, D. J. Radack, and A. Serbeto, in *Proceedings of the 9th International Free Electron Laser Conference*, Williamsburg, VA, Sept. 14–18, 1987 [Nucl. Instrum. Methods (to be published)].
[21]J. K. Burton, J. J. Condon, W. H. Lupton, F. L. Desrosier, A. C. Greenwald, J. M. Henness, M. J. Rhee, and G. T. Zorn, IEEE Trans. Nucl. Sci. **NS-20**, 321 (1973).